Terahertz Quantum Cascade Lasers
and Real-time T-rays Imaging at video rate

Qing Hu

Department of Electrical Engineering and Computer Science,

Massachusetts Institute of Technology, Cambridge, MA 02139, U.S.A.

Email: qhu@mit.edu

Abstract: We report our development of terahertz (THz) quantum-cascade lasers with record performance. Using those high-power lasers as the illumination sources and a focal-plane array camera, we are able to perform real-time THz imaging at video rate.

Keywords: Terahertz, quantum-cascade lasers, imaging

1. Introduction

Terahertz (1-10 *THz*, $\hbar\omega$ = 4-40 *meV*, and λ = 30-300 *μm*) frequencies are among the most underdeveloped electromagnetic spectra, even though their potential applications are promising in detection of chemical and biological agents, imaging for medical and security applications, astrophysics, plasma diagnostics, end-point detection in dry etching processes, remote atmospheric sensing and monitoring, noninvasive inspection of semiconductor wafers, high-bandwidth free-space communications, and ultrahigh-speed signal processing[1]. This underdevelopment is primarily due to the lack of coherent solid-state THz sources that can provide high radiation intensities (greater than one *mW*) and continuous-wave (CW) operations. This is because the THz frequency falls between two other frequency ranges in which conventional semiconductor devices have been well developed. One is the microwave and millimeter-wave frequency range, and the other is the near-infrared and optical frequency range. Semiconductor electronic devices that utilize freely moving electrons (such as transistors, Gunn oscillators, Schottky-diode frequency multipliers, and photomixers) are limited by the transit time and parasitic *RC* time constants. Consequently, the power level of these electronic devices decreases as $1/f^4$, or even faster, as the frequency f increases above 1 *THz*. Semiconductor photonic devices based on quantum-mechanical interband transitions (such as bipolar laser diodes), however, are limited to frequencies higher than those corresponding to the semiconductor energy gap, which is higher than 10 *THz* even for narrow-gap lead-salt materials. Thus, the frequency range of 1-10 *THz* is inaccessible for conventional semiconductor devices.

Semiconductor quantum wells are human-made quantum-mechanical systems in which the

energy levels can be designed and engineered to be of any value.   Consequently, unipolar lasers based on intersubband transitions (electrons that make lasing transitions between subband levels) were proposed for long-wavelength sources as early as the 1970s[2] .This device concept has been realized in the successful development of quantum-cascade lasers (QCL) at mid-infrared wavelengths[3].Since then, impressive improvements in performance have been made in terms of power levels, operating temperatures, and frequency characteristics at mid-infrared frequencies.

In contrast to the remarkable development of mid-infrared QCLs, the development of THz QCLs below the *Reststrahlen* band (~8-9 *THz* in GaAs) turned out to be much more difficult than initially expected, because of two unique challenges at THz frequencies. First, the energy level separations that correspond to THz frequencies are quite narrow (~10 *meV*). Thus, the selective depopulation mechanism based on energy-sensitive LO-phonon scattering, which has been successfully implemented in mid-infrared QCLs, is not applicable. Second, mode confinement, which is essential for any laser oscillation, is difficult to achieve at THz frequencies. Conventional dielectric-waveguide confinement is not applicable because the evanescent field penetration, which is proportional to the wavelength and is on the order of several tens of microns, is much greater than the active gain medium of several microns.

In October 2001, almost eight years after the initial development of QCLs, the first QCL operating at 4.4 *THz*, below the *Reststrahlen* band, was developed[4]. This laser was based on a chirped superlattice structure that had been successfully developed at mid-infrared frequencies. Mode confinement in this THz QCL was achieved using a double-surface plasmon waveguide grown on a semi-insulating (SI) GaAs substrate. Shortly after this breakthrough, a THz QCL based on bound-to-continuum intersubband transition was developed at ~3.4 *THz* [5].

Our group has pursued a different approach to achieve lasing at THz frequencies. We have investigated possibilities of using fast LO-phonon scattering to depopulate the lower radiative level [6-8] and using double-sided metal waveguides for THz mode confinement[9]. After an extensive investigation, these efforts finally bore fruits. In November 2002, a 3.4-*THz* QCL was developed in which the depopulation of the lower radiative level was achieved through resonant LO-phonon scattering [10].The performance of this laser device is promising, especially its operating temperatures. One of the laser devices was operated in the pulse mode up to 87 *K*, above liquid-nitrogen temperature [11]. When fabricated with the double-sided metal-metal waveguides, THz QCLs based on similar quantum-well structures have demonstrated the highest pulsed operating temperature of ~170 *K*, the highest CW operating temperature of 117 *K*, and the longest wavelength of ~188 *μm*. Using a high-power THz QCL and a 240×320 focal-plane array camera, we are now able to perform real-time THz imaging at video rate, that is, taking movies in "T-rays". These rapid developments indicate great potentials for THz QCLs in various applications. In the following sections, we summarize key results of these investigations [10-36].

2. THz gain medium based on resonant LO-phonon scattering for depopulation

The unipolar intersubband lasers are known to yield a high value of gain, because of a large joint density of states as a result of the two subbands tracking each other in the k-space; thus electrons emit photons at the same energy regardless of their initial momentum. Consequently, the peak gain is related to the inverted population density Δn_{3D} in a simple linear fashion:

$$g_{peak} = \Delta n_{3D} \frac{e^2 \omega}{\pi \hbar \varepsilon_r^{1/2} \varepsilon_o c_o} \frac{z_{ij}^2}{\Delta f} = \Delta n_{3D} \frac{e^2}{2\pi \varepsilon_r^{1/2} \varepsilon_o c_o m^*} \frac{f_{ij}}{\Delta f} \qquad (1)$$

$$\approx 67 \left(\Delta n_{3D}/10^{15} cm^{-3}\right) \frac{f_{ij}}{\Delta f / THz} \, cm^{-1}.$$

In Eq. (1), Δn_{3D} is the three-dimensional inverted population density in the active region. $z_{ij} = \langle i|z|j \rangle$ is the dipole moment and $f_{ij} = (2m^*\omega z_{ij}^2)/\hbar$ is the dimensionless oscillator strength of the $i{\rightarrow}j$ transition. Δf is the FWHM linewidth of spontaneous emission in units of Hz (but in units of THz in the last numerical part of Eq. (1)). Clearly from Eq. (1), there are only **three** parameters that determine the peak material gain, Δn, Δf, and f_{ij}. All the other parameters are either fundamental constants or material parameters that are not subject to engineering and manipulation. In our structures, the measured spontaneous emission linewidth is typically ~1 *THz* (~4 *meV*). We need to mostly concentrate on the optimization of two parameters, Δn and f_{ij}.

The first successful THz QCLs were designed around chirped superlattice structures[4],which are characterized by large oscillator strengths. However, the depopulation of the lower lasing level relies on resonant tunneling and electron-electron scattering, which could suffer from thermal backfilling because of narrow subband separations within the miniband of a superlattice. The direct use of LO-phonon scattering for depopulation of the lower state offers several distinctive advantages. First, when a collector (ground) state is separated from the lower lasing level by at least the LO-phonon energy $\hbar\omega_{LO}$(=36 *meV* = 9 *THz*), depopulation can be extremely fast, and it does not depend much on temperature or the electron distribution. Second, the large energy separation provides intrinsic protection against thermal backfilling of the lower radiative state. Both properties are important in allowing higher temperature operation of lasers with high output power levels.

While fast scattering out of the lower lasing level is necessary to achieve population inversion, a long upper-state lifetime τ_u is also highly desirable to increase the level of population inversion. Our previous designs addressed this problem by making the optical transition diagonal (i.e., between states in adjacent wells), so as to reduce upper-state overlap with the collector state [6].However, this resulted in a small oscillator strength, and in a broad emission linewidth due to

interface roughness. A second design featured a vertical radiative transition[7],which improved the radiative overlap and had a relatively narrow linewidth (~2 *meV* ≈ 0.5 *THz*), but depopulation was nonselective and slow, due to the thick barrier needed to reduce parasitic scattering from the upper state.

The key element in the present design is to use resonant LO-phonon scattering to selectively depopulate the lower radiative level while maintaining a long upper level lifetime, and it resulted in a breakthrough success. Fig. 1 shows the conduction band profile and subband wavefunctions under the designed bias of 64*mV/module*. Each module contains four quantum wells, shown inside the dashed box, and 175 such modules are connected in series to form the quantum cascade laser. Under this bias, the electrons are injected from the injector level 1' to the upper lasing level 5 through resonant tunneling. The radiative transition between levels 5 and 4 is spatially vertical, yielding a relatively large oscillator strength (f_{54} ≈ 0.96). The depopulation is highly selective and fast, as only the lower level 4 is at resonance with a level 3 in the adjacent well, where fast LO-phonon scattering (τ_4 ≈ 0.5 *ps*) takes place to empty electrons in levels 3 and 4 to the injector doublet 1 and 2. The scattering time of the upper level 5 to the ground states 2 and 1, due to a relatively thick barrier, is quite long ($\tau_{5\rightarrow2,1}$ ≈ 7 *ps*), which is important to maintain a population inversion between levels 5 and 4. Electrons in level 1 are then injected to level 5 of the following module (not shown here), completing the cascade pumping scheme.
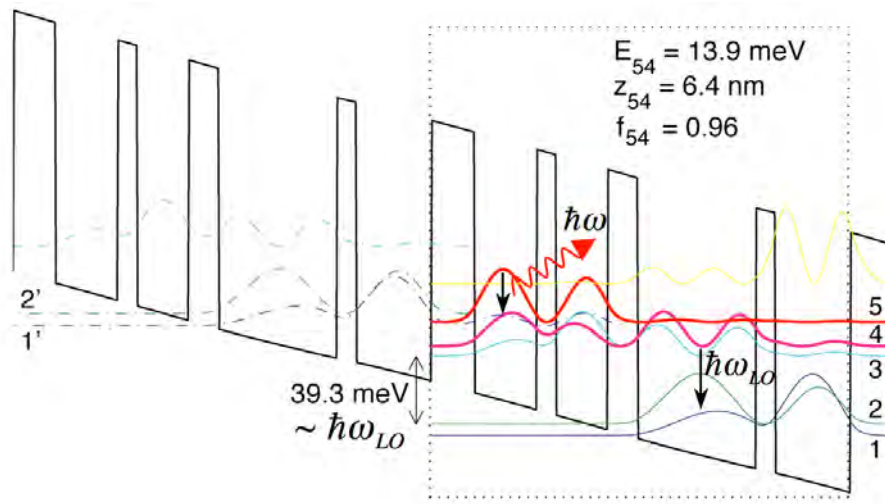

Fig1. Conduction band profile calculated using a self-consistent Schrödinger and Poisson solver biased at 64*mV/module*.

Mode confinement in this laser device was achieved using a double-surface plasmon waveguide formed between the top metallic contact and the bottom heavily doped GaAs layer, as in the case of other THz QCLs[4]. Lasing was obtained in this device and the emission frequency of 3.4 *THz* corresponds to a photon energy of 14.2 *meV*, close to the calculated value of 13.9 *meV*. Pulsed lasing operation from devices fabricated from this first laser wafer is observed up to 87 *K*[11].

3. THz mode confinement using double-side metal waveguides

Because of the amphoteric nature of silicon dopants in GaAs materials, the maximum attainable electron density is approximately $5 \times 10^{18}/cm^3$. At this carrier concentration, the penetration depth is on the order of 1 *μm* at THz frequencies, causing a significant cavity loss if the lower side of the mode confinement is provided by heavily doped GaAs layers. The first successful development of THz QCLs utilized a double surface plasmon layer grown on semi-insulating GaAs substrate for mode confinement. This structure is easy to grow and fabricate, and it provides adequate mode confinement for most of the THz QCLs. However, the mode confinement factor Γ in this scheme is far below unity ($\Gamma \sim 0.2$-0.5 for reported lasers).

Following our initial success in developing the 3.4-*THz* laser, we demonstrated the first terahertz QCL that uses a double-sided metal-metal waveguide for mode confinement[13]. This metal-semiconductor-metal structure is essentially the same as the microstrip transmission lines that are widely used for waveguiding at microwave and millimeter-wave frequencies, and the geometry is compatible with the TM polarization of intersubband transitions. Due to the shallow skin depth in the metal (several hundred Å), the waveguide can be made with very low losses and a confinement factor close to unity. Our current THz lasers with metal-metal waveguide were fabricated using copper-to-copper wafer bonding followed by substrate removal. The schematic of the bonding and substrate removal process is illustrated in Fig. 2.
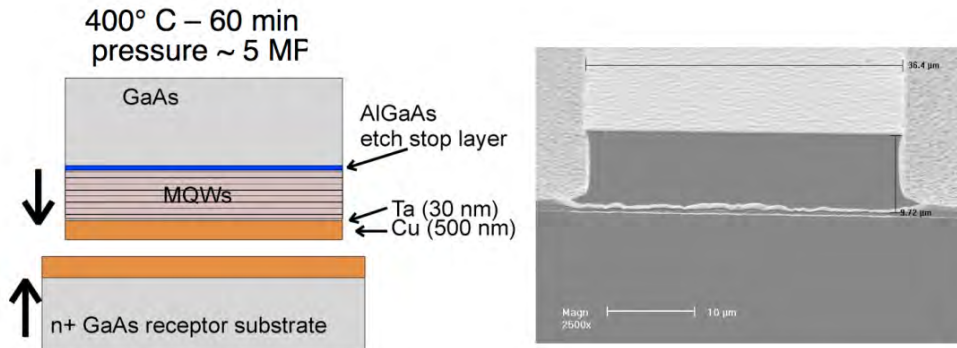

Fig.2. Left: Schematic of the wafer bonding process for double-side metal-metal waveguide.   Right: A SEM picture of the fabricated device.

Based on this metal-metal waveguide structure and using improved gain media that reduced the lasing threshold current densities, we have achieved several records in the performance of THz QCLs. These include but not limited to: the highest pulsed operating temperature of ~169 *K*, the first CW THz QCL operating above the important liquid nitrogen temperature of 77 *K* ($T_{max} = $ 117 *K*).

In addition to the record performance in operating temperatures and wavelength, we have recently developed high-power THz quantum-cascade lasers that produce ~250 *mW* of power, as

shown in Fig. 4. Using these high-power lasers, we are now able to perform THz imaging in real time at a video rate of ~20 frames/second, that is, making movies in T-rays.
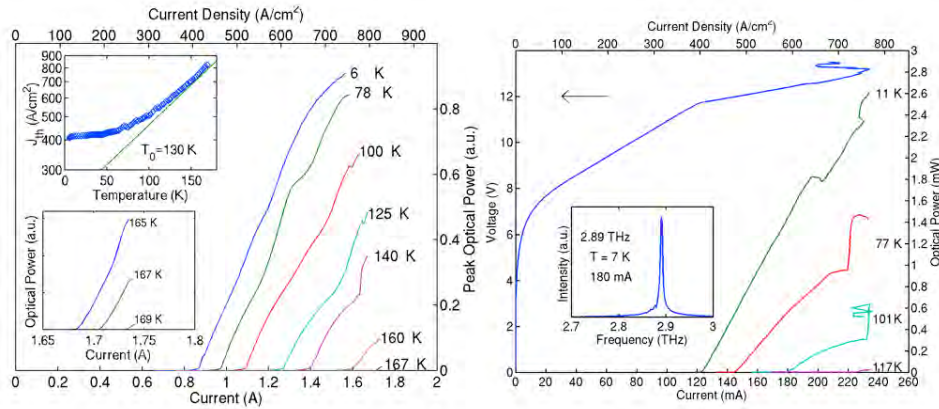

Fig.3 Left: Pulsed power-current and voltage-current relations measured up to ~169 *K* heatsink temperature. Right: CW power-current and voltage-current relations measured up to ~117 *K* heatsink temperature. The inset shows the CW voltage-current and differential resistance-current relations of the device.
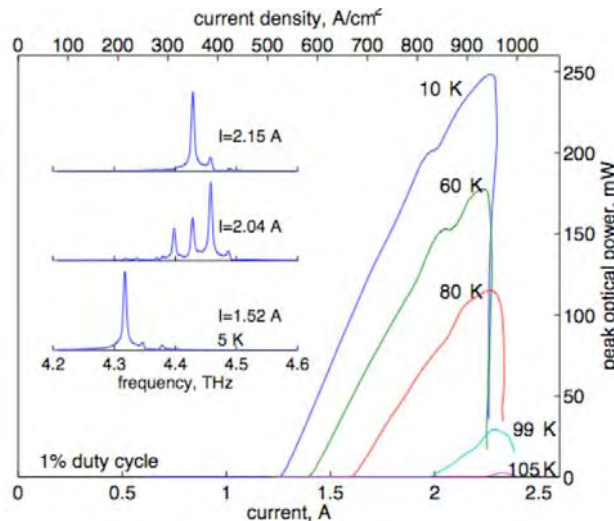

Fig.4 A ~4.4-*THz* quantum-cascade laser with peak power level of ~250 *mW*.

4. Real-time THz imaging using QCLs and focal-plane array cameras

Imaging using radiation in the terahertz frequency range, 0.3 *THz* to 10 *THz*, has demonstrated the ability to see the details within visibly opaque objects such as integrated circuits packages, leaves, teeth, thin tissue samples, and illicit drugs in envelopes. The vast majority of THz imaging has been done by linearly scanning an object through a tightly focused THz beam – a practice which limits the acquisition time to the mechanical scan rate of the system. With upper limits of 100's of pixels/second for mechanical scanning, a complete image takes minutes to acquire.

Real-time imaging (~30 frames per second or more) has previously been demonstrated by using an electro-optic crystal for frequency upconversion so that THz images can be viewed with a CCD focal-plane camera.   However, this setup requires precise timing of the optical and THz pulses, necessitating a scanning delay mechanism, adding to its complexity.   Furthermore, because of the short THz pulses (<1 *ps*), this scheme is inherently broadband (>1 *THz*).   In applications such as the drug detection scheme, where detection of narrow-band fingerprint is required, a coherent narrow-band illumination source is crucial.   Because of their compact sizes, many THz quantum-cascade lasers with different frequencies, corresponding to different chemical absorption bands, can be packaged tightly, forming a frequency agile coherent radiation source. In combination with a focal-plane imager, such a system can perform frequency-sensitive THz imaging at a rate far greater than the previous methods, allowing real-time THz monitoring and screening.

In this work, real-time, continuous wave (CW) terahertz imaging is demonstrated for the first time using THz QCLs and a focal-plane array camera.   The experimental arrangement is shown in Fig. 5. The terahertz QCL is cooled by a cryogen-free pulsed-tube thermomechanical cooler, produces ~50 *mW* of power at ~30 *K*. As shown in the figure, imaging experiments in both transmission and reflection mode can be performed. Since the microbolometer camera was initially designed for the 10-μm wavelength range for night-vision applications, we developed a differential scheme to subtract the strong ambient background at ~300 *K* and reduce $1/f$ noise[34].
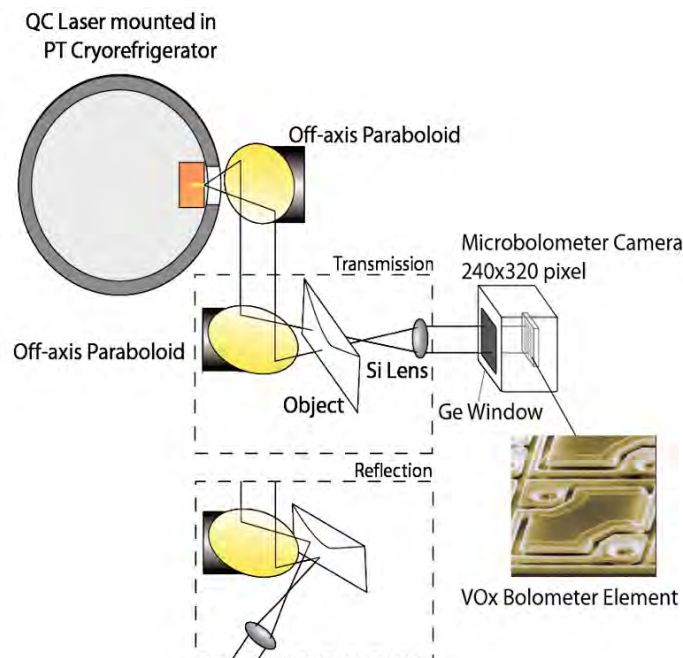

Fig.5 Experimental setup of the THz imaging system. The photo shows a vanadium oxide microbolometer (Courtesy of BAE Systems, Lexington, MA).   Cutaway depicts alternate reflection mode setup.

An example of the real-time imaging experiment is shown in Fig. 6, in which several hand-written characters inside a regular mail envelope are clearly visible in THz imaging, in both transmission and reflection mode. It should be pointed out that this particular imaging application cannot be done at other frequencies: x-rays lack contrast; millimeter-waves do not provide sufficient spatial resolution; and infrared radiation is heavily scattered and/or absorbed by fibrous materials. While these still images are recognizable, when they are viewed in real-time the integration of the eye and pattern recognition of the brain aid tremendously as seen in real-time video. With additional QCL's the system will allow analytic, real-time multi-frequency imaging. Very recently, by carefully designing and fabricating QCLs with the desired frequency characteristics, we have demonstrated real-time, long-range (>25 meters), transmission mode imaging [36]. This demonstration is a necessary step towards the ultimate goal of a standoff imaging system.
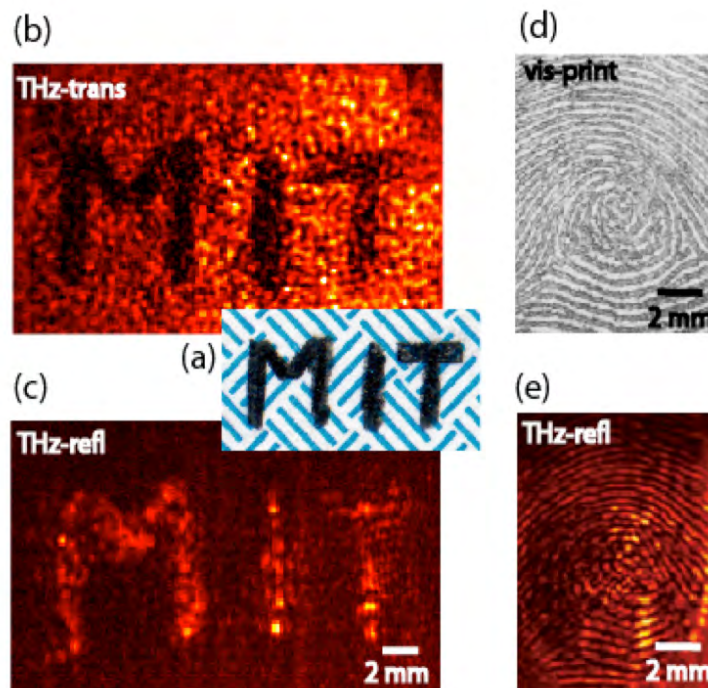

Fig.6 Pencil letters written on the inside of a paper security envelope at visible frequencies (a), in THz transmission mode (b, 1 frame, 1/20 second) and THz reflection mode (c, 20 frames, 1 second).   Visible frequency thumb print (d), and THz reflection mode image the thumb of the leading author (e, 20 frames).

Acknowledgment

References

[1] Special issue on "The terahertz gap: the generation of far-infrared radiation and its applications," *Phil. Trans. Royal Society of London,* A362, 195-414, (2004).

[2] R. F. Kazarinov and R. A. Suris, "Possibility of amplification of electromagnetic waves in a semiconductor with a superlattice," *Sov. Phys. Semicond.* 5, 707, (1971).

[3] J. Faist, F. Capasso, D. L. Sivco, C. Sirtori, A. L. Hutchinson, and A. Y. Cho, "Quantum cascade laser," *Science* 264, 477, (1994).

[4] R. Köhler, A. Tredicucci, F. Beltram, H. E. Beere, E. H. Linfield, A. G. Davies, D. A. Ritchie, R. C. Iotti, and F. Rossi, "Terahertz semiconductor-heterostructure laser," *Nature,* 417, 156, (2002).

[5] G. Scalari, L. Ajili, J. Faist, H. Beere, G. Davies, E. Linfield, and D. Ritchie, "Far infrared (≈86 μm) quantum-cascade lasers based on bound-to-continuum transition with operation temperature up to 90 K," *Appl. Phys. Lett.* 82, 3165, (2003).

[6] B. Xu, Q. Hu, and M. R. Melloch, " Electrically Pumped Tunable Terahertz Emitter Based on Intersubband Transition," *Appl. Phys. Lett.* 71, 440, (1997).

[7] Williams, B. S., B. Xu, Q. Hu, and M. R. Melloch, "Narrow-linewidth Terahertz Intersubband Emission from Three-level Systems," *Appl. Phys. Lett.* 75, 2927, (1999).

[8] B. S. Williams and Q. Hu, "Optimized energy separation for phonon scattering in three-level terahertz intersubband lasers," *J. Appl. Phys.* 90, 5504, (2001).

[9] B. Xu, Ph.D. thesis, "Development of Intersubband Terahertz Lasers Using Multiple Quantum Well Structures," MIT, unpublished, (1998).

[10] B. S. Williams, H. Callebaut, S. Kumar, Q. Hu, and J. L. Reno, "3.4-THz quantum cascade laser based on LO-phonon scattering for depopulation," *Appl. Phys, Lett.* 82, 1015, (2003).

[11] B. S. Williams, S. Kumar, H. Callebaut, Q. Hu, and J. L. Reno, "3.4 THz quantum cascade laser operating above liquid nitrogen temperature," *Electro. Lett.* 39, 915, (2003).

[12] H. Callebaut, S. Kumar, B. S. Williams, and J. L. Reno, "Analysis of transport and thermal properties of THz quantum cascade lasers," *Appl. Phys. Lett.* 83, 207, (2003).

[13] B. S. Williams, S. Kumar, H. Callebaut, Q. Hu, and J. L. Reno, "Terahertz quantum cascade laser at λ ≈ 100 μm using metal waveguide for mode confinement," *Appl. Phys. Lett.* 83, 2124, (2003).

[14] Q. Hu, B. S. Williams, S. Kumar, H. Callebaut, and J. L. Reno, "Terahertz quantum cascade lasers based on resonant phonon scattering for depopulation," *Phil. Trans. R. Soc. London,* A362, 233-249 (2004).

[15] B. S. Williams, S. Kumar, H. Callebaut, Q. Hu, and J. L. Reno, "Terahertz Quantum Cascade Lasers Operating up to 137 K," *Appl. Phys. Lett.* 83, 5142, (2003).

[16] H. Callebaut, S. Kumar, B. S. Williams, Q. Hu, and J. L. Reno, "Importance of electron-impurity scattering for electron transport in THz quantum-cascade lasers," *Appl. Phys. Lett.* 84, 645, (2004).

[17] S. Kumar, B. S. Williams, S. Kohen, Q. Hu, and J. L. Reno, "Continuous-wave operation of terahertz

quantum-cascade lasers above liquid-nitrogen temperature," *Appl. Phys. Lett.* 84, 2494, (2004).

[18] B. S. Williams, S. Kumar, Q. Hu, and J. L. Reno, "Resonant-phonon terahertz quantum-cascade laser operating at 2.1 THz (λ ≈ 141 µm)," *Elect. Lett.* 40, 431, (2004).

[19] Q. Hu, B. S. Williams, S. Kumar, H. Callebaut, S. Kohen, and J. L. Reno, "Resonant-phonon-assisted THz Quantum Cascade Lasers with Metal-metal Waveguides," a Topical Issue on TERAHERTZ TECHNOLOGY, *Journal of Semiconductor Science and Technology*, 20, S228-S236, (2005).

[20] S. Kohen, B. S. Williams, and Q. Hu, "Electromagnetic modeling of terahertz quantum cascade laser waveguides and resonators," *J. Appl. Phys.* 97, 053106, (2005).

[21] M. S. Vitiello, G. Scamarcio, B. S. Williams, S. Kumar, Q. Hu, and J. L. Reno, "Measurement of subband electronic temperatures and population inversion in THz quantum cascade lasers," *Appl. Phys. Lett.* 86, 111115, (2005).

[22] J. R. Gao, J. N. Hovenier, Z. Q. Yang, J. J. A. Baselmans, A. Baryshev, M. Majenius, T. M. Klapwijk, A. J. L. Adam, T. O. Klassen, B. S. Williams, S. Kumar, Q. Hu, and J. L. Reno, "A terahertz heterodyne receiver based on a quantum cascade laser and a superconducting bolometer," *Appl. Phys. lett.* 86, 244104, (2005).

[23] H. C. Liu, M. Wächter, D. Ban, Z. R. Wasilewski, M. Buchanan, G. C. Aers, J. C. Cao, S. L. Feng, B. S. Williams, and Q. Hu, "Effect of doping concentration on the performance of terahertz quantum-cascade lasers," *Appl. Phys. Lett.* 87, 141102, (2005).

[24] L. Betz, R. T. Boreiko, B. S. Williams, S. Kumar, Q. Hu, and J. L. Reno, "Frequency and Phaselock Control of a 3-THz Quantum Cascade Laser," *Opt. Lett.* 30, 1837, (2005).

[25] W. M. Lee and Q. Hu, "Real-Time, Continuous-Wave Terahertz Imaging using a Microbolometer Focal-Plane Array," *Opt. Lett.* 30, 2563 (2005). Also reported in *Opto&Laser Europe*, page 14, December, (2005).

[26] S. Williams, S. Kumar, Q. Hu, and J. L. Reno, "Operation of terahertz quantum-cascade lasers at 164 K in pulsed mode and at 117 K in continuous-wave mode," *Optics Express*, 13, 3331-3339, (2005).

[27] S. Williams, S. Kumar, Q. Hu, and J. L. Reno, "Distributed-feedback terahertz quantum-cascade lasers using laterally corrugated metal waveguides," *Opt. Lett.* 30, 2909, (2005).

[28] H. Callebaut and Q. Hu, "Importance of coherence for electron transport in terahertz quantum cascade lasers," J. Appl. 98, 104505, (2005).

[29] E. Orlova, J. N. Hovenier, T. O. Klaassen, I. Kasalynas, A. J. L. Adam, A. Baryshev, J. R. Gao, T. M. Klapwijk, B. S. Williams, S. Kumar, Q. Hu, and J. L. Reno, "Antenna model for wire lasers," *Phys. Rev. Lett.* 96, 173904, (2006).

[30] B. S. Williams, S. Kumar, Q. Hu, and J. L. Reno, "High-power terahertz quantum-cascade lasers," *Elect. Lett.* 42, 89 (2006).

[31] J.L. Adam, I. Kašalynas, J.N. Hovenier, T.O. Klaassen, J.R. Gao, E.E. Orlova, B.S. Williams, S. Kumar, Q. Hu, and J. L. Reno, "Beam pattern of Terahertz quantum cascade lasers with sub-wavelength cavity dimensions," *Appl. Phys. Lett.* 88, 151105, (2006).

[32] S. Kumar, B. S. Williams, Q. Hu, and J. L. Reno, "1.9-THz quantum-cascade lasers with one-well injector," *Appl. Phys. Lett.* 88, 121123, (2006).

[33] Baryshev, J. N. Hovenier, A. J. L. Adam, I. Kasalynas, J. R. Gao, T. O. Klaassen, B. S. Williams, S. Kumar, Q. Hu, and J. L. Reno, "Phase-lock and free-running linewidth of a two-mode terahertz quantum cascade laser," *Appl. Phys.* Lett. 89, 031115, (2006).

[34] Alan W.M. Lee, Benjamin S. Williams, Sushil Kumar, Qing Hu, and John L. Reno, "Real-Time Imaging using a 4.3-THz Quantum Cascade Laser and a 320×240 Microbolometer Focal-Plane Array," *IEEE Photonics Technology Letters* 18, 1415, (2006).

[35] B. S. Williams, S. Kumar, Q. Qin, Q. Hu, and J. L. Reno, "Terahertz quantum cascade lasers with double resonant-phonon depopulation," *Appl. Phys. Lett.* 88, 261101, (2006).

[36] Alan W.M. Lee, Qi Qin, Sushil Kumar, Benjamin S. Williams, Qing Hu, and John L. Reno, 'Real-Time Terahertz Imaging over a Standoff Distance (>25 meters)," *Appl. Phys. Lett.* 89, 141125, (2006).